Nano Energy 44 (2018) 15–22

Contents lists available at ScienceDirect

Nano Energy

journal homepage: www.elsevier.com/locate/nanoen

Communication

Dynamic imaging of metastable reaction pathways in lithiated cobalt oxide electrodes

Qianqian Li[a,b,d,1], Jinsong Wu[a,b,*,1], Zhenpeng Yao[a,1], Yaobin Xu[a], Michael M. Thackeray[c], Chris Wolverton[a], Vinayak P. Dravid[a,b,*]

[a] Department of Materials Science and Engineering, Northwestern University, Evanston, IL 6020, USA
[b] NUANCE Center, Northwestern University , Evanston, IL 60208, USA
[c] Electrochemical Energy Storage Department, Chemical Sciences and Engineering Division, Argonne National Laboratory, IL 60439, USA
[d] Materials Genome Institute, Shanghai University, Shanghai, PR China

ARTICLE INFO

Keywords:
Metastable phase transformations
In-situ transmission electron microscopy
In-situ lithiation
Conversion reaction electrode
Lithium-ion battery
DFT calculation

ABSTRACT

Understanding how lithium-ion batteries function down to the atomic level during charge and discharge cycling can provide valuable guidance to optimize structure-property relationships and to design and understand new electrode materials. Lithium insertion and reactions with the electrodes during charge and discharge cycling can occur *via* metastable structures with complex ordering and related non-equilibrium phenomena. Remarkably, these processes remain still poorly understood despite their significance in the operation of lithium battery systems in critical technologies. In this communication, we present the dynamics of lithium insertion into Co_3O_4 and the evolution of metastable phases as probed by *in-situ* transmission electron microscopy, in concert with first principles density functional theory calculations. We show that the initial lithium *intercalation* reaction occurs with the formation of several metastable and intermediate phases, followed by a sequence of *conversion* reactions that perturb and expand the cubic-close-packed oxygen array, ultimately generating an end-product of finely dispersed cobalt metal clusters within a Li_2O matrix. The calculated non-equilibrium lithiation pathways corroborate with the experimental lithiation voltages, and explain the significant hysteresis that occurs during electrochemical cycling. The data provide new insights into the complexity of solid state lithium electrochemistry in metal oxides that are relevant to advancing lithium battery technology.

1. Introduction

Lithium insertion reactions contribute significantly to the electrochemical performance of Li-ion batteries that currently dominate the world's growing rechargeable battery industry, while conversion reactions hold significant promise for the next generation batteries, due to their large capacities [1–4]. Despite intensive research in this field since the commercialization of the first C/$LiCoO_2$ battery products, there is limited information about the electrochemical processes that occur at the atomic- and nano-scale in electrode structures, particularly the transient formation of intermediate and metastable configurations that have insufficient time to relax and equilibrate [5,6]. Metastable configurations can exist only for a short time span under these dynamic conditions, which makes it extremely difficult to measure them experimentally. Such configurations will impact battery performance, *e.g.,* capacity, cyclability and voltage hysteresis. Recent advances in developing TEM techniques [7–15] have allowed real-time, *in-operando*, visualization of dynamic electrochemical processes in lithium-ion battery materials with atomic resolution. Density functional theory (DFT) calculations serve as a complementary tool to experiments, and allow us to predict atomistic structural models of metastable lithiation pathways, which can be validated by comparison of simulated and experimental high resolution images.

Traditional Li-ion battery electrodes, such as layered $LiCoO_2$ [16,17] and substituted analogues, *e.g.*, $LiNi_{0.33}Mn_{0.33}Co_{0.33}O_2$ [18], the spinel $LiMn_2O_4$ [19,20] and $Li_4Ti_5O_{12}$ [21,22], and olivine $LiFePO_4$ [23] operate by insertion reactions alone, sometimes with a phase change; they typically release and re-accommodate between 0.5 and 1.0 Li^+ ions per transition metal ion. The reactions are typically accompanied by concomitant redox of the transition metal ions between divalent and tetravalent oxidation states during charge and discharge, thereby limiting the delivered electrode capacity to about 100 − 170 mA h/g. On the other hand, conversion reactions that occur when metal oxides are extensively lithiated involve the reduction of

* Corresponding authors at: Department of Materials Science and Engineering, Northwestern University, Evanston, IL 6020, USA.
E-mail addresses: jinsong-wu@northwestern.edu (J. Wu), v-dravid@northwestern.edu (V.P. Dravid).
[1] These authors contributed equally to this work.

https://doi.org/10.1016/j.nanoen.2017.11.052
Received 26 October 2017; Received in revised form 22 November 2017; Accepted 22 November 2017
Available online 28 November 2017

metal ions to the metallic state and their displacement from the oxide host. [2,4,24,25] Despite cycling stability and hysteresis limitations, these reactions are appealing because they can involve more than one Li per transition metal, and hence yield significantly higher capacities, *e.g.*, 700–800 mA h/g, at relatively low potentials *vs.* metallic lithium, providing an opportunity to exploit metal oxide conversion materials as anodes for high energy lithium-ion battery systems.

The reaction of lithium with cobalt oxides and iron oxides, such as Co_3O_4, CoO, Fe_3O_4, Fe_2O_3, $LiFeO_2$, and $LiFe_5O_8$ at room temperature and high temperature (400 °C) was first disclosed more than 30 years ago [3,25–30]. Lithiation of Co_3O_4 at room temperature occurs first by an insertion process to form an intermediate rock salt phase, $LiCo_3O_4$, before metallic cobalt is extruded from the structure [3]; in this case, the reaction can be formulated simplistically as:

$$Co_3O_4 \xrightarrow{+Li} LiCo_3O_4 \xrightarrow{+7Li} 3\ Co + 4\ Li_2O \quad (1)$$

A severe hysteresis (~ 1.0 V) has been observed in the voltage/capacity plot of cycled $Li/Li_xCo_3O_4$ cells [24]. The hysteresis results in a low energy efficiency on each cycle, which has prohibited the use of Co_3O_4, notably as an anode, in practical lithium-ion cells. The exact reasons for the large hysteresis remain unclear despite many studies of this phenomenon. Several hypotheses, based on experimental and computational studies, have been proposed such as 1) ohmic drop [31], 2) nanosize effects [32,33], 3) surface chemistries and reactions [34,35], 4) compositional inhomogeneity [8,31], and 5) asymmetric reaction pathways during charge and discharge [36,37]. The contribution to hysteresis from points 1, 2 and 3 above are generally considered to be small ($0.1 < V < 0.4$) [31–35], whereas the hysteresis originating from point 4 should be largely alleviated when the particle size is reduced, enabling fast reaction kinetics. It appears that hysteresis effects are generally independent of the morphology and shape of the electrode particles, as emphasized by studies on nanotubes, nanowires and hollow nanospheres of Co_3O_4 [38–40]. As we demonstrate here, the substantial discrepancy between thermodynamic and kinetic reaction paths can account for a large voltage hysteresis (> 1.0 V) in transition metal oxides like Co_3O_4. Yu et al. [36] identified an intermediate phase during the conversion from $LiTiS_2$ to $Cu_{0.5}TiS_2$ while the re-conversion reaction exhibits simple two-phase features without any intermediate phase. Chang et al. [37] found similar reaction path difference between the charge and discharge of Cu_2Sb. In this paper, we explore, by both theoretical and *in-situ* experimental (TEM) methods, the complex electrochemical lithiation of Co_3O_4 electrodes during an initial discharge. This combined approach, with strong correlations between experiment and theory, provides further evidence that the production of intermediate and metastable phases plays a significant role in the hysteresis of electrochemical metal-displacement reactions.

Specifically, we have studied the room temperature, electrochemical discharge behavior of Co_3O_4 nanocrystals decorated on highly conductive multi-wall carbon nanotubes (CNTs). Co_3O_4 was selected as a model system because it provides the opportunity to study in detail, by *in situ* TEM, both insertion and conversion reaction processes in one material and to observe directly the nanoparticle lithiation process in real-time and at the atomic scale. A density functional theory (DFT) based approach was developed to predict the initial lithium insertion reaction and corresponding metastable phases that were observed and verified experimentally. The proposed DFT methodology provides an explanation for the significant polarization observed in the voltage profile of Co_3O_4, and for conversion reactions conducted at room-temperature, in general. While most of the Co_3O_4 nanoparticles show an obvious intercalation stage, one nanoparticle, in particular, appeared to skip the intercalation stage, reacting immediately by a conversion process, thereby, highlighting the complexity and non-uniformity of the electrochemical lithiation process.

2. Material and methods

2.1. Nanocomposite preparation

Co_3O_4/CNT nanocomposites were synthesized by hydrothermal method similar to that previously reported[41,42]. In a typical experiment, 200 mg cobalt (III) acetate tetrahydrated and 15 mg carbon nanotube were dissolved in a 20 mL solution of dimethylformamide and water with a 8:2 volume ratio by magnetic stirring for 30 min. The solution was subsequently loaded into a Teflon-lined autoclave (25 mL capacity). The stainless steel autoclave was sealed and heated to 120 °C for 2 h. Thereafter, the autoclave was cooled to room temperature, the precipitates collected by filtration after being repeatedly washed with ethanol and deionized water, and finally dried in an oven at 60 °C.

2.2. In situ TEM experiments

A nanobattery design was built inside TEM by using the nanofactory STM-TEM holder, which can provide a positive/negative bias between two electrodes in the circuit. Co_3O_4/CNT was adhered to one end of Au rod using a conductive epoxy, which acted as the working electrode. Lithium scratched directly by a tungsten rod was used as the counter electrode. Two electrodes of the nanobattery were placed in contact with each other inside the transmission electron microscope using a precisely controlled piezo-motor with a movement resolution of ~ 1 nm. The bias range of the STM-TEM holder, namely, − 10 V to + 10 V, is more than adequate to drive lithium ions from the lithium source to react with the active Co_3O_4 particles. In our experiments, a negative bias range of − 0.5 to − 2.5 V was applied during the lithiation process, and a positive + 3 to + 4 V was applied to the circuit on delithiation. The electron dosage was carefully monitored in the experiments to minimize its effect on the current observations.

The cell consisted of a Li metal foil anode, passivated by a Li^+-conducting solid electrolyte layer, produced by briefly exposing the Li metal anode to air prior to assembly, and a nanoparticulate Co_3O_4 cathode. Although the composition of the protective layer is unknown at this stage, we speculate that it was likely comprised of Li_2CO_3, LiOH, Li_2O, Li_3N and/or other lithium-containing species.

2.3. Density functional theory calculations

The first principle calculations were carried out in the Vienna Ab-initio Simulation Package (VASP) [43–46] with the projector augmented wave (PAW) potentials [47]. The generalized gradient approximation (GGA) of Perdew-Becke-Ernzerhof (PBE) was used for the exchange-correlation functional with spin polarization always included. A plane-wave basis set cutoff energy of 520 eV and Γ-centered k-meshes with the density of 8000 k-points per reciprocal atom were used in all calculations. DFT + U method was used to treat Co-3d states with a U value of 3.3 eV adopted following previous studies [48–51].

2.4. Non-equilibrium phase searching (NEPS) through the Li-Co_3O_4 reaction

To simulate the metastable lithiation process of the Co_3O_4, we applied a structure-based non-equilibrium phase searching (NEPS) method [52–55]. We first built a model with a supercell of Co_3O_4 containing 6 Co ions (4 Co^{3+}, 2 Co^{2+}) and 8 O^{2-} ions, which has 16 total tetrahedral and octahedral unoccupied sites that Li^+ ions can insert (Fig. 5). To investigate the energetic influence of the Co migration, [3] three initial structures (Fig. S7) were created with none/half/all of the Co ions moved from tetrahedral sites (T_d) to the octahedral sites (O_h). For the Co ions migrated configuration, we reproduce the partially ordered structure using the special quasi-random structure (SQS) method. An SQS was generated based on a Monte Carlo algorithm implemented in ATAT [56–59] with the constraint that the pair and

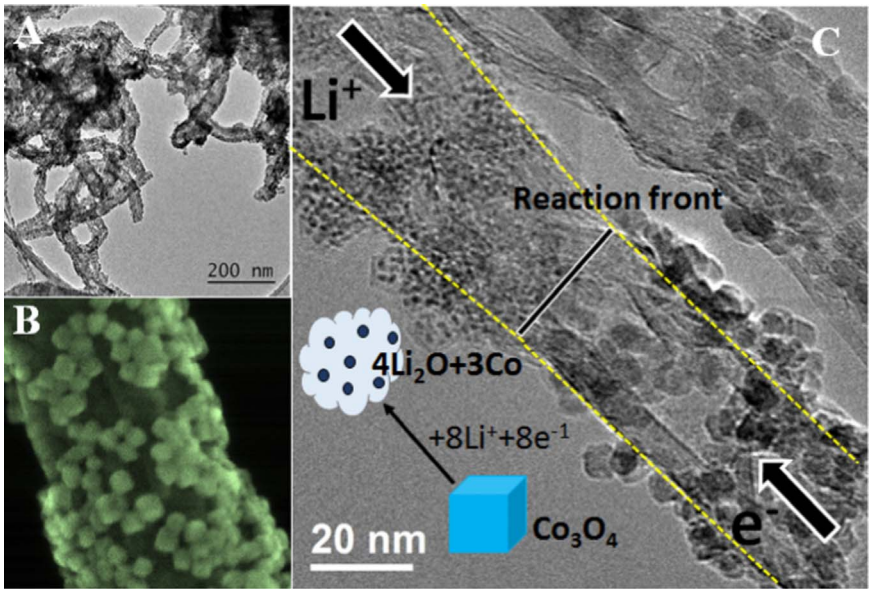

Fig. 1. Co_3O_4 nanocubes on a carbon nanotube (CNT) and a lithiated product. (A) Low-magnification TEM image and (B) SEM images of Co_3O_4 nanocubes on CNT. (C) *In-situ* high resolution electron microscopy (HREM) image showing the electrically-induced disintegration of lithiated Co_3O_4 particles into metallic cobalt (black dots) in a surrounding Li_2O matrix.

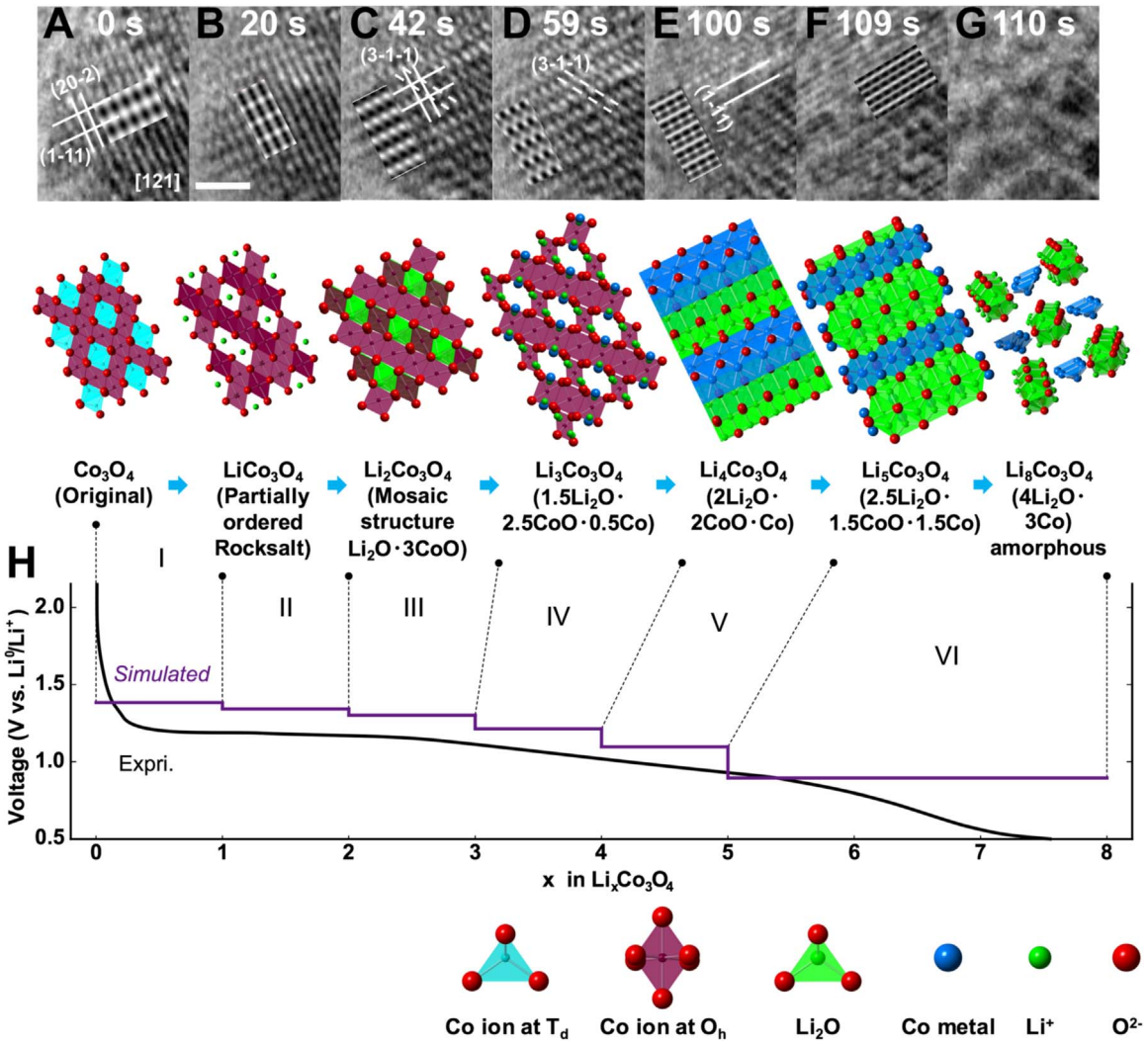

Fig. 2. *In-situ* HREM lithiation of a Co_3O_4 nanoparticle at relatively low lithiation speed. (A)–(G) upper row: HREM images of the lithiation process as a function of time (seconds). Simulated HREM images are inserted to highlight crystallographic indices of the planes. (A)–(G) Low-row: structural models of lithium-inserted phases, from Co_3O_4 to $Li_8Co_3O_4$, predicted by DFT simulations. The structural model is oriented along the same direction as the [121] Co_3O_4. The scale bar is 1 nm. (H) Simulated voltage profile of Co_3O_4 through the metastable phases, compared to experimental voltage profile adapted from Ref. [41].

triplet correlation functions of the SQS are identical to those of the statistically random Co/vacancy population of cation sites at least up to the third nearest neighbor. Starting from these structures shown in Fig. S8, we inserted the Li atom(s) into the unoccupied octahedral and tetrahedral site(s) for a range of compositions within $0 < x \leq 8$ for $Li_xCo_3O_4$. For each composition, we generated all symmetrically-distinct configurations of Li on these sites. [60–62] Electrostatic energies for these structures were then calculated taking into account the nominal charge states for the ions in the system [63]. Afterward, the structures at each composition were ranked by the electrostatic energies and the two lowest energy structures are further relaxed using DFT (Fig. S7b). Convex hulls were built with all formation energies of different stoichiometries. Voltage profiles were calculated using the energetics of the phases on the hull.

3. Results and discussion

Fig. 1A and B show TEM and SEM images of Co_3O_4 nanocubes, approximately 5 nm in dimension, grown hydrothermally on the surface of multi-wall CNTs. Electron diffraction confirmed the *fcc* spinel symmetry of the Co_3O_4 crystallites (F*d*-3*m*). A miniature lithium half-cell for the *in-situ* TEM experiments was assembled, as described in Fig. S1. The cell was discharged by applying a potential bias of approximately − 3 V to induce lithiation of the Co_3O_4 particles. Video S1 shows a live TEM recording of the electrochemical lithiation of Co_3O_4 nanocubes, while eight screen shots from this video (Fig. S2) highlight morphological changes that occur to the nanocubes.

Supplementary material related to this article can be found online at http://dx.doi.org/10.1016/j.nanoen.2017.11.052.

Fig. 2 shows high resolution electron microscopy (HREM) screenshot images from Video S2 as a function of reaction time (t) together with simulated representations of $Li_xCo_3O_4$ structures for various values of x ($0 \leq x \leq 8$). The HREM images provide a visual picture of the structural changes that occur progressively on lithiation (Fig. S3). During the initial lithiation from t = 0 to t = 20 s (stage I), the crystal lattice remains largely intact while the volume of the nanocube expands by approximately 8% from ~ 63 nm^3 to ~ 68 nm^3. This finding is in excellent agreement with DFT calculations that predict that the incorporation of one Li^+ ion into Co_3O_4 to form a lithiated spinel (rock salt) $LiCo_3O_4$ structure would induce a volume expansion of 7.86% (Tables S1 and S2); these calculations were used to simulate HREM images (Figs. S4–S6) as an aid to index the lattice planes in the experimentally-derived TEM images. During stage I, lithium insertion displaces cobalt ions from the tetrahedral (8a) sites of the spinel structure into neighboring octahedral (16c) sites, while the incoming lithium ions occupy the remaining interstitial 16c octahedral sites, thereby generating a rock salt configuration in a two-phase reaction, consistent with prior X-ray diffraction analyses [20]. Here, we assume that the Li and Co ions are disordered over the 16c octahedral sites, as reported previously [6]. Computationally, such a disordered structure provides a lower potential (1.39 V) than an ordered structure (1.64 V), consistent with the experimental voltage profile shown in Fig. 2 and Fig. S9).

Supplementary material related to this article can be found online at http://dx.doi.org/10.1016/j.nanoen.2017.11.052.

During stage II of the reaction, *i.e.*, t ≈ 42 to t ≈ 98 s in Video S2, the introduction of additional lithium results in a stronger contrast in the lattice fringes of the (3-1-1) planes of the parent Co_3O_4 structure (Fig. 2C,D). After reaction with two Li^+ ions, *i.e.*, at the composition $Li_2Co_3O_4$ (or alternatively, $Li_2O{\cdot}3CoO$), all the cobalt ions would be divalent, suggesting that this composition is the upper limit for lithium uptake prior to the reduction of divalent cobalt to the metallic state (Co^0). The existence of overlithiated $Li_xCo_3O_4$ compounds ($0 < x \leq 2$), first postulated in 1985 by Thackeray and Baker et al. [3] for x = 1.07, 1.47 and 1.92, can be rationalized in terms of a mosaic structure, in which localized configurations with CoO-, Li_2O- or intermediate CoO-Li_2O character exist, depending on the extent of lithiation of the localized regions. The transformation of a crystalline- to a mosaic structure is not surprising, given the significant differences in the lattice parameters of $LiCo_3O_4$, CoO and Li_2O structures and their atomic configurations. Indeed, our DFT calculations predict that overlithiating $LiCo_3O_4$ to $Li_2Co_3O_4$ ($Li_2O{\cdot}3CoO$) occurs with the partial migration of octahedrally-coordinated cobalt ions in $LiCo_3O_4$ to tetrahedral sites in $Li_2Co_3O_4$ (Fig. 2C). This finding corroborates a previously-reported X-ray diffraction analysis of a chemically-prepared, overlithiated $Li_{1.92}Co_3O_4$ sample that provided evidence of both tetrahedrally- and octahedrally-coordinated cobalt in the structure [3]. We believe that the presence of lattice streaks along the (3-1-1) plane in the experimental HREM images (Fig. 2(C,D)) reflects the onset of these highly complex structural changes and the generation of localized Li_2O, CoO and fully reduced Co metal configurations.

At lithiation stage III (t = 100 to t = 109 s) in Fig. 2(E,F), {111} lattice fringes, corresponding to a significantly expanded *fcc* lattice are clearly present, consistent with the production of reduced, CoO-like configurations in an extensively lithiated structure. The HREM images and theoretical simulations of extensively lithiated $Li_xCo_3O_4$ structures suggest that, during this stage of the reaction, the displacement of cobalt atoms during their reduction to the metallic state may be responsible for the significant expansion of the lattice (perpendicular to the {111} planes), yielding a convoluted structure composed of Co^0 and CoO slabs alternating with slabs of Li_2O (see Fig. 2E, F for idealized representations of the structures). During the final stage of the reaction, stage IV, that occurs approximately one second later at t = 110 s (Fig. 2G and S3), there is an instantaneous pulverization of the crystalline structure, induced by the reduction and extrusion of the remaining cobalt from the CoO slabs, and the clustering of cobalt atoms within a surrounding Li_2O matrix, as depicted in Fig. 1C and by the simulated, thermodynamically relaxed and fully lithiated crystal structure, $Li_8Co_3O_4$ ($4Li_2O{\cdot}3Co$), in Fig. 2G. The calculated (open circuit) overall value of the voltages of the Li/Co_3O_4 cell, based on the

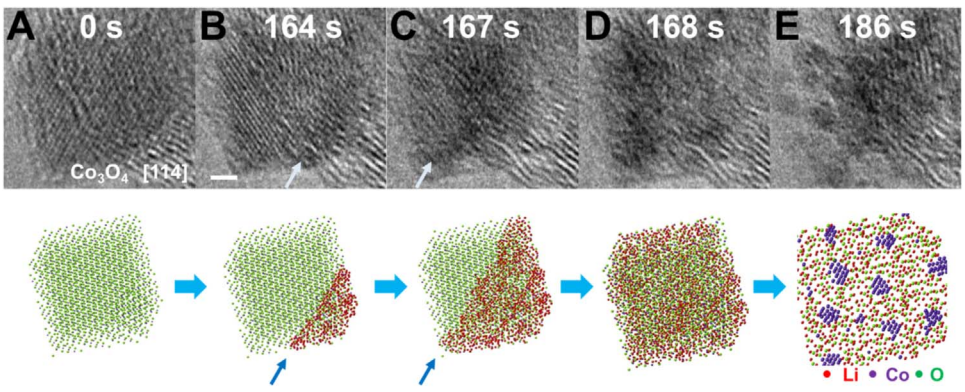

Fig. 3. *In-situ* HREM lithiation of a Co_3O_4 nanoparticle at relatively fast lithiation speed. (A)-(G) Top: HREM images of the lithiation process as a function of time (seconds). Bottom: Illustration of the lithiation process. In about 4 s, a lithiated Co_3O_4 nanoparticle transforms from a crystalline phase into a composite of Co^0-clusters embedded in a Li_2O matrix. Co: purple; O: Green; Li: Red. The scale bar is 1 nm.

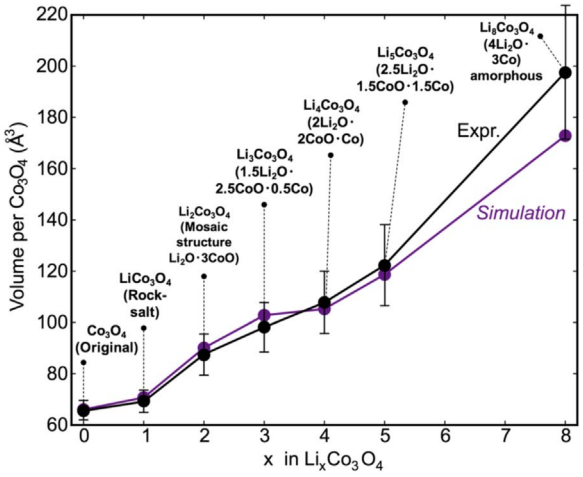

Fig. 4. Normalized volumetric expansion of Co_3O_4 nanoparticles during lithiation. Normalized volumes of a Co_3O_4 nanoparticle lithiated relatively slowly as a function of Li amount (circles).

metastable structures in Fig. 2H, is in much better agreement with experimental lithiation (black curve) than the calculated equilibrium voltage (See Supporting information Section I-C). The tendency for Co_3O_4 nanoparticles [38–40] to generate a sloping voltage profile rather than a flat voltage plateau [4] is interesting because it implies that particle size also influences the reaction mechanism and pathway. In general, the trend and shape of the calculated equilibrium voltage profile is similar to the curve of the experimental lithiation reaction, suggesting that the lithiation process follows an energetic pathway close to the equilibrium reaction. Based on this evidence, we conclude that the large hysteresis in Li/Co_3O_4 cells can be attributed, at least in part, to asymmetric reaction paths during lithiation (discharge) and delithiation (charge) (Fig. S9), consistent with the predictions by Yu et al. [36] and Chang et al. [37] and the strong correlation between the calculated volume and measured values of the lithiated Co_3O_4 structures that are generated during discharge (Fig. 4). Such an intercalation reaction stage with appearance of intermediate phases have also been observed in other Co_3O_4 nanoparticles as shown in Figs. S11 and S12. By carefully do HREM simulation (as shown in supplementary figure Fig. S13), there is about ~ 1.8° tilting of the [121] Co_3O_4 nanoparticle (Fig. 2a) along the [11-1] direction, although its influence to the identification of the phases is small and can be neglected.

A second Co_3O_4 nanoparticle showed significantly different lithiation behavior (Fig. S10). Snapshots of this nanoparticle (Fig. 3(A–E) from Video S3**),** originally oriented close to the [114] zone axis, indicate that the morphological features and volume did not change substantially until the nanoparticle had been lithiated for 164 s. We tentatively attribute the apparent low reactivity to poor contact of the Co_3O_4 nanoparticle with the underlying CNT backbone that would suppress electronic conductivity and electrochemical lithiation. Video S3 clearly shows that, within 4–8 s beyond t = 164, lithium insertion and conversion reactions occur almost simultaneously and extremely quickly to yield cobalt metal clusters within a Li_2O matrix; the surface expands significantly, while the reaction continues into the bulk, as shown in Video S3 (t = 169 to t = 207 s). The 'two-phase' process that occurs as the reaction front progresses through a single nanoparticle is represented schematically and sequentially below the images in

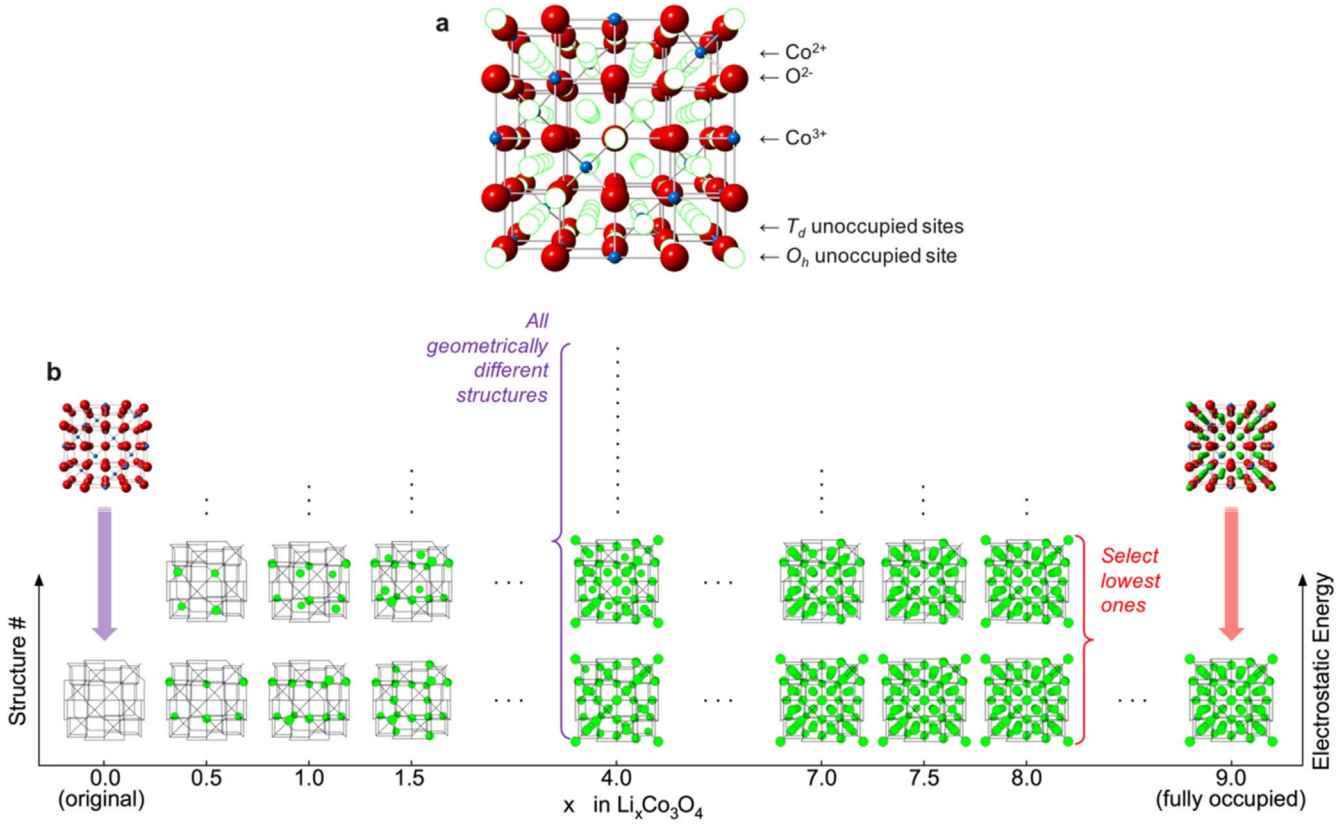

Fig. 5. Search for the metastable structures through the Li-Co_3O_4 reaction. The searching process proceeds as follows: (i) Possible insertion sites (T_d and O_h) were identified from the original Co_3O_4 spinel structure. (ii) All symmetrically-distinct configurations of Li on the unoccupied sites were generated for each composition using Enum (Li/vacancy orderings are shown by the green circles with the Co_3O_4 structure visualized by lines). (iii) Total energies of all the configurations generated were sampled using electrostatic calculations. (iv) For each composition, corresponding structures were ranked by the total energies, and the three lowest energy structures were further relaxed using DFT. The formation energies for these selected structures were then evaluated. (v) Using formation energies obtained, the non-equilibrium Li-Co_3O_4 convex hull is built. The composition points located on the convex hull then correspond to the identified non-equilibrium phases.

Fig. 3A–E. It is clear that the stage of intercalation reaction can be greatly shorten as the lithiation speed increase. Although we did not observe the metastable and intermediate phases in the fast-lithiated nanoparticle, the existence of similar intercalation reaction stage could not be completely excluded due to the limits of current experimental setting, such as the limit of temporal resolution of the CCD camera (~ 5 frame per second) (Fig.s 4 and 5).

Supplementary material related to this article can be found online at http://dx.doi.org/10.1016/j.nanoen.2017.11.052.

4. Conclusions

In summary, the combination of experimental *in-situ* TEM data and DFT theoretical calculations have provided further insight into conversion reactions that occur in lithiated metal oxide electrode materials of relevance to lithium battery technology. Observations, analyses and predictions have revealed highly complex reaction processes involving intermediate and metastable phases during the lithiation of the $Li_xCo_3O_4$ electrode system. The study highlights, in particular, the need for new approaches to design unique structures that will simplify and control conversion reaction pathways and minimize hysteresis effects, thereby improving the electrochemical properties of this class of electrodes.

Acknowledgements

This work was supported as part of the Center for Electrochemical Energy Science, an Energy Frontier Research Center funded by the U.S. Department of Energy (DOE), Office of Science, Basic Energy Sciences under Award # DEAC02-06CH11357, and the Initiative for Sustainability and Energy at Northwestern (ISEN). This work was also supported by the NU*ANCE* Center at Northwestern University, using the EPIC facility that receives support from the Soft and Hybrid Nanotechnology Experimental (SHyNE) Resource (NSF NNCI-1542205); the MRSEC program (NSF DMR-1121262) at the Materials Research Center; the International Institute for Nanotechnology (IIN); the Keck Foundation; and the State of Illinois, through the IIN. MMT was funded by the DOE Office of Vehicle Technologies where complementary research on Li-Co-Ni-O spinels is being undertaken. Nanocomposite samples were prepared by Professor Junming Xu at Hangzhou Dianzi University, China. We acknowledge the computing resources from: 1) the National Energy Research Scientific Computing Center, a DOE Office of Science User Facility supported by the Office of Science of the U.S. Department of Energy under Contract DE-AC02-05CH11231. 2) Blues, a high-performance computing cluster operated by the Laboratory Computing Resource Center at Argonne National Laboratory.

Appendix A. Supporting information

Supplementary data associated with this article can be found in the online version at http://dx.doi.org/10.1016/j.nanoen.2017.11.052.

References

[1] M. Armand, J.-M. Tarascon, Building Better Batteries, Nature 451 (2008) 652–657, http://dx.doi.org/10.1038/451652a.
[2] P. Poizot, S. Laruelle, S. Grugeon, L. Dupont, J.M. Tarascon, Nano-sized transition-metal oxides as negative-electrode materials for lithium-ion batteries, Nature 407 (2000) 496–499, http://dx.doi.org/10.1038/35035045.
[3] M. Thackeray, S. Baker, K. Adendorff, J. Goodenough, Lithium insertion into Co3O4: a preliminary investigation, Solid State Ion. 17 (1985) 175–181, http://dx.doi.org/10.1016/0167-2738(85)90069-4.
[4] F. Badway, I. Plitz, S. Grugeon, S. Laruelle, M. Dolle, A.S. Gozdz, J.-M. Tarascon, Metal oxides as negative electrode materials in Li-ion cells, Electrochem. Solid-State Lett. 5 (2002) A115–A118, http://dx.doi.org/10.1149/1.1472303.
[5] A. Singer, A. Ulvestad, H.-M. Cho, J.W. Kim, J. Maser, R. Harder, Y.S. Meng, O.G. Shpyrko, Nonequilibrium structural dynamics of nanoparticles in LiNi(1/2)Mn (3/2)O4 cathode under operando conditions, Nano Lett. 14 (2014) 5295–5300, http://dx.doi.org/10.1021/nl502332b.
[6] M.Z. Bazant, Theory of chemical kinetics and charge transfer based on nonequilibrium thermodynamics, Acc. Chem. Res. 46 (2013) 1144–1160, http://dx.doi.org/10.1021/ar300145c.
[7] J.Y. Huang, L. Zhong, C.M. Wang, J.P. Sullivan, W. Xu, L.Q. Zhang, S.X. Mao, N.S. Hudak, X.H. Liu, A. Subramanian, H. Fan, L. Qi, A. Kushima, J. Li, In situ observation of the electrochemical lithiation of a single SnO_2 nanowire electrode, Science 330 (2010) 1515–1520, http://dx.doi.org/10.1126/science.1195628.
[8] C.-M. Wang, In situ transmission electron microscopy and spectroscopy studies of rechargeable batteries under dynamic operating conditions: a retrospective and perspective view, J. Mater. Res. 30 (2015) 326–339, http://dx.doi.org/10.1557/jmr.2014.281.
[9] B.L. Mehdi, J. Qian, E. Nasybulin, C. Park, D.A. Welch, R. Faller, H. Mehta, W.A. Henderson, W. Xu, C.M. Wang, J.E. Evans, J. Liu, J.-G. Zhang, K.T. Mueller, N.D. Browning, Observation and quantification of nanoscale processes in lithium batteries by operando electrochemical (S)TEM, Nano Lett. 15 (2015) 2168–2173, http://dx.doi.org/10.1021/acs.nanolett.5b00175.
[10] K. He, H.L. Xin, K. Zhao, X. Yu, D. Nordlund, T.-C. Weng, J. Li, Y. Jiang, C.A. Cadigan, R.M. Richards, M.M. Doeff, X.-Q. Yang, E.A. Stach, J. Li, F. Lin, D. Su, Transitions from near-surface to interior redox upon lithiation in conversion electrode materials, Nano Lett. 15 (2015) 1437–1444, http://dx.doi.org/10.1021/nl5049884.
[11] J. Li, K. He, Q. Meng, X. Li, Y. Zhu, S. Hwang, K. Sun, H. Gan, Y. Zhu, Y. Mo, E.A. Stach, D. Su, Kinetic PHase Evolution of Spinel Cobalt Oxide during Lithiation, ACS Nano 10 (2016) 9577–9585, http://dx.doi.org/10.1021/acsnano.6b04958.
[12] M.T. McDowell, S.W. Lee, J.T. Harris, B.A. Korgel, C. Wang, W.D. Nix, Y. Cui, In situ TEM of two-phase lithiation of amorphous silicon nanospheres, Nano Lett. 13 (2013) 758–764, http://dx.doi.org/10.1021/nl3044508.
[13] L. Luo, J. Wu, J. Xu, V.P. Dravid, Atomic resolution study of reversible conversion reaction in metal oxide electrodes for lithium-ion battery, ACS Nano. 8 (2014) 11560–11566, http://dx.doi.org/10.1021/nn504806h.
[14] K. He, S. Zhang, J. Li, X. Yu, Q. Meng, Y. Zhu, E. Hu, K. Sun, H. Yun, X.-Q. Yang, Y. Zhu, H. Gan, Y. Mo, E.A. Stach, C.B. Murray, D. Su, Visualizing non-equilibrium lithiation of spinel oxide via in situ transmission electron microscopy, Nat. Commun. 7 (2016) 11441, http://dx.doi.org/10.1038/ncomms11441.
[15] F. Wang, H.-C. Yu, M.-H. Chen, L. Wu, N. Pereira, K. Thornton, A. Van der Ven, Y. Zhu, G.G. Amatucci, J. Graetz, Tracking lithium transport and electrochemical reactions in nanoparticles, Nat. Commun. 3 (2012) 1201–1208, http://dx.doi.org/10.1038/ncomms2185.
[16] J.B. Goodenough, Evolution of strategies for modern rechargeable batteries, Acc. Chem. Res. 46 (2013) 1053–1061, http://dx.doi.org/10.1021/ar2002705.
[17] K. Mizushima, P.C. Jones, P.J. Wiseman, J.B. Goodenough, LixCoO2 (0 < x < 1): a new cathode material for batteries of high energy density, Mater. Res. Bull. 15 (1980) 783–789, http://dx.doi.org/10.1016/0025-5408(80)90012-4.
[18] N. Yabuuchi, Y. Koyama, N. Nakayama, T. Ohzuku, Solid-state chemistry and electrochemistry of LiCo1/3Ni1/3Mn1/3O2 for advanced lithium-ion batteries, J. Electrochem. Soc. 152 (2005) A1434–A1440, http://dx.doi.org/10.1149/1.1924227.
[19] M.M. Thackeray, W.I.F. David, P.G. Bruce, J.B. Goodenough, Lithium insertion into manganese spinels, Mater. Res. Bull. 18 (1983) 461–472, http://dx.doi.org/10.1016/0025-5408(83)90138-1.
[20] R.J. Gummow, A. de Kock, M.M. Thackeray, Improved capacity retention in rechargeable 4 V lithium/lithium-manganese oxide (spinel) cells, Solid State Ion. 69 (1994) 59–67, http://dx.doi.org/10.1016/0167-2738(94)90450-2.
[21] K.M. Colbow, J.R. Dahn, R.R. Haering, Structure and electrochemistry of the spinel oxides LiTi2O4 and Li43Ti53O4, J. Power Sources 26 (1989) 397–402, http://dx.doi.org/10.1016/0378-7753(89)80152-1.
[22] E. Ferg, R.J. Gummow, A. de Kock, M.M. Thackeray, Spinel anodes for lithium-ion batteries, J. Electrochem. Soc. 141 (1994) L147–L150, http://dx.doi.org/10.1149/1.2059324.
[23] A.K. Padhi, K.S. Nanjundaswamy, J.B. Goodenough, Phospho-olivines as positive-electrode materials for rechargeable lithium batteries, J. Electrochem. Soc. 144 (1997) 1188–1194, http://dx.doi.org/10.1149/1.1837571.
[24] D. Larcher, G. Sudant, J.-B. Leriche, Y. Chabre, J.-M. Tarascon, The electrochemical reduction of Co3O4 in a lithium cell, J. Electrochem. Soc. 149 (2002) A234–A241, http://dx.doi.org/10.1149/1.1435358.
[25] J. Cabana, L. Monconduit, D. Larcher, M.R. Palacín, Beyond intercalation-based Li-ion batteries: the state of the art and challenges of electrode materials reacting through conversion reactions, Adv. Mater. 22 (2010) E170–E192, http://dx.doi.org/10.1002/adma.201000717.
[26] M.M. Thackeray, W.I.F. David, J.B. Goodenough, Structural characterization of the lithiated iron oxides LixFe3O4 and LixFe2O3, Mater. Res. Bull. 17 (1982) 785–793, http://dx.doi.org/10.1016/0025-5408(82)90029-0.
[27] M.M. Thackeray, S.D. Baker, J. Coetzer, The electrochemical behaviour of Co3O4 and CoO cathodes in high-temperature cells, Mater. Res. Bull. 17 (1982) 405–411, http://dx.doi.org/10.1016/0025-5408(82)90092-7.
[28] M.M. Thackeray, W.I.F. David, J.B. Goodenough, High-temperature lithiation of α-Fe2O3: a mechanistic study, J. Solid State Chem. 55 (1984) 280–286, http://dx.doi.org/10.1016/0022-4596(84)90278-0.
[29] N.A. Godshall, I.D. Raistrick, R.A. Huggins, Thermodynamic investigations of ternary lithium-transition metal-oxygen cathode materials, Mater. Res. Bull. 15 (1980) 561–570, http://dx.doi.org/10.1016/0025-5408(80)90135-X.
[30] L.A. De Picciotto, M.M. Thackeray, Lithium insertion into the spinel LiFe5O8, Mater. Res. Bull. 21 (1986) 583–592, http://dx.doi.org/10.1016/0025-5408(86)90113-3.
[31] L. Li, R. Jacobs, P. Gao, L. Gan, F. Wang, D. Morgan, S. Jin, Origins of large voltage

hysteresis in high-energy-density metal fluoride lithium-ion battery conversion electrodes, J. Am. Chem. Soc. 138 (2016) 2838–2848, http://dx.doi.org/10.1021/jacs.6b00061.
[32] G. Rollmann, M.E. Gruner, A. Hucht, R. Meyer, P. Entel, M.L. Tiago, J.R. Chelikowsky, Shellwise mackay transformation in iron nanoclusters, Phys. Rev. Lett. 99 (2007) 083402–083405, http://dx.doi.org/10.1103/PhysRevLett.99.083402.
[33] R.E. Doe, K.A. Persson, Y.S. Meng, G. Ceder, First-principles investigation of the Li − Fe − F phase diagram and equilibrium and nonequilibrium conversion reactions of iron fluorides with lithium, Chem. Mater. 20 (2008) 5274–5283, http://dx.doi.org/10.1021/cm801105p.
[34] R. Khatib, A.-L. Dalverny, M. Saubanère, M. Gaberscek, M.-L. Doublet, Origin of the voltage hysteresis in the CoP conversion material for Li-ion batteries, J. Phys. Chem. C 117 (2013) 837–849, http://dx.doi.org/10.1021/jp310366a.
[35] D. Meggiolaro, G. Gigli, A. Paolone, P. Reale, M.L. Doublet, S. Brutti, Origin of the voltage hysteresis of MgH2 electrodes in lithium batteries, J. Phys. Chem. C 119 (2015) 17044–17052, http://dx.doi.org/10.1021/acs.jpcc.5b04615.
[36] H.-C. Yu, C. Ling, J. Bhattacharya, J.C. Thomas, K. Thornton, A. Van der Ven, Designing the next generation high capacity battery electrodes, Energy Environ. Sci. 7 (2014) 1760–1768, http://dx.doi.org/10.1039/c3ee43154a.
[37] D. Chang, M.-H. Chen, A. Van der Ven, Factors contributing to path hysteresis of displacement and conversion reactions in Li ion batteries, Chem. Mater. 27 (2015) 7593–7600, http://dx.doi.org/10.1021/acs.chemmater.5b02356.
[38] X.W. Lou, D. Deng, J.Y. Lee, J. Feng, L.A. Archer, Self-supported formation of needlelike Co3O4 nanotubes and their application as lithium-ion battery electrodes, Adv. Mater. 20 (2008) 258–262, http://dx.doi.org/10.1002/adma.200702412.
[39] Y. Li, B. Tan, Y. Wu, Freestanding mesoporous quasi-single-crystalline CO3O4 nanowire arrays, J. Am. Chem. Soc. 128 (2006) 14258–14259, http://dx.doi.org/10.1021/ja065308q.
[40] X. Wang, X.-L. Wu, Y.-G. Guo, Y. Zhong, X. Cao, Y. Ma, J. Yao, Synthesis and lithium storage properties of Co3O4 nanosheet-assembled multishelled hollow spheres, Adv. Funct. Mater. 20 (2010) 1680–1686, http://dx.doi.org/10.1002/adfm.200902295.
[41] J. Xu, J. Wu, L. Luo, X. Chen, H. Qin, V. Dravid, S. Mi, C. Jia, Co3O4 nanocubes homogeneously assembled on few-layer graphene for high energy density lithium-ion batteries, J. Power Sources 274 (2015) 816–822, http://dx.doi.org/10.1016/j.jpowsour.2014.10.106.
[42] Q. Li, J. Wu, J. Xu, V.P. Dravid, Synergistic sodiation of cobalt oxide nanoparticles and conductive carbon nanotubes (CNTs) for sodium-ion batteries, J. Mater. Chem. A 4 (2016) 8669–8675, http://dx.doi.org/10.1039/C6TA02051H.
[43] G. Kresse, J. Hafner, Ab initio molecular dynamics for liquid metals, Phys. Rev. B 47 (1993) 558–561, http://dx.doi.org/10.1103/PhysRevB.47.558.
[44] G. Kresse, J. Hafner, Ab initio molecular-dynamics simulation of the liquid-metal-amorphous-semiconductor transition in germanium, Phys. Rev. B 49 (1994) 14251–14269, http://dx.doi.org/10.1103/PhysRevB.49.14251.
[45] G. Kresse, J. Furthmüller, Efficiency of ab-initio total energy calculations for metals and semiconductors using a plane-wave basis set, Comput. Mater. Sci. 6 (1996) 15–50, http://dx.doi.org/10.1016/0927-0256(96)00008-0.
[46] G. Kresse, J. Furthmüller, Efficient iterative schemes for ab initio total-energy calculations using a plane-wave basis set, Phys. Rev. B 54 (1996) 11169–11186, http://dx.doi.org/10.1103/PhysRevB.54.11169.
[47] P.E. Blöchl, Projector augmented-wave method, Phys. Rev. B 50 (1994) 17953–17979, http://dx.doi.org/10.1103/PhysRevB.50.17953.
[48] S.L. Dudarev, S.Y. Savrasov, C.J. Humphreys, A.P. Sutton, G.A. Botton, S.Y. Savrasov, C.J. Humphreys, A.P. Sutton, Electron-energy-loss spectra and the structural stability of nickel oxide: an LSDA + U study, Phys. Rev. B 57 (1998) 1505–1509, http://dx.doi.org/10.1103/PhysRevB.57.1505.
[49] J. Chen, X. Wu, A. Selloni, Electronic structure and bonding properties of cobalt oxide in the spinel structure, Phys. Rev. B 83 (2011) 245204–245210, http://dx.doi.org/10.1103/PhysRevB.83.245204.
[50] J. Chen, A. Selloni, Electronic states and magnetic structure at the Co3O4 (110) surface: a first-principles study, Phys. Rev. B 85 (2012) 085306–085314, http://dx.doi.org/10.1103/PhysRevB.85.085306.
[51] L. Wang, T. Maxisch, G. Ceder, Oxidation energies of transition metal oxides within the GGA + U framework, Phys. Rev. B 73 (2006) 195107–195112, http://dx.doi.org/10.1103/PhysRevB.73.195107.
[52] Z. Yao, S. Kim, M. Aykol, Q. Li, J. Wu, J. He, C. Wolverton, Revealing the conversion mechanism of transition metal oxide electrodes during lithiation from first-principles, Chem. Mater. (2017), http://dx.doi.org/10.1021/acs.chemmater.7b02058.
[53] Q. Li, Z. Yao, J. Wu, S. Mitra, S. Hao, T.S. Sahu, Y. Li, C. Wolverton, V.P. Dravid, Intermediate phases in sodium intercalation into MoS2 nanosheets and their implications for sodium-ion batteries, Nano Energy 38 (2017) 342–349, http://dx.doi.org/10.1016/j.nanoen.2017.05.055.
[54] H. Liu, Q. Li, Z. Yao, L. Li, Y. Li, C. Wolverton, M.C. Hersam, V.P. Dravid, Origin of fracture-resistance to large volume change in Cu-doped Co3O4 electrode, Adv. Mater. (2017), http://dx.doi.org/10.1002/adma.201704851.
[55] K. He, Z. Yao, S. Hwang, N. Li, K. Sun, H. Gan, Y. Du, H. Zhang, C. Wolverton, D. Su, Kinetically-driven phase transformation during lithiation in copper sulfide nanoflakes, Nano Lett. 17 (2017) 5726–5733, http://dx.doi.org/10.1021/acs.nanolett.7b02694.
[56] E. Cockayne, A. van de Walle, Building effective models from sparse but precise data: application to an alloy cluster expansion model, Phys. Rev. B 81 (2010) 012104–012107, http://dx.doi.org/10.1103/PhysRevB.81.012104.
[57] A. van de Walle, Multicomponent multisublattice alloys, nonconfigurational entropy and other additions to the alloy theoretic automated toolkit, Calphad 33 (2009) 266–290.
[58] A. van de Walle, A complete representation of structure-property relationships in crystals, Nat. Mater. 7 (2008) 455–458.
[59] H. Bin, Z. Yao, S. Zhu, C. Zhu, H. Pan, Z. Chen, C. Wolverton, D. Zhang, A high-performance anode material based on FeMnO3/graphene composite, J. Alloy. Compd. 695 (2017) 1223–1230, http://dx.doi.org/10.1016/j.jallcom.2016.10.249.
[60] G. Hart, R. Forcade, Algorithm for generating derivative structures, Phys. Rev. B 77 (2008) 224115–224126, http://dx.doi.org/10.1103/PhysRevB.77.224115.
[61] G.L.W. Hart, R.W. Forcade, Generating derivative structures from multilattices: algorithm and application to hcp alloys, Phys. Rev. B 80 (2009) 014120–014127, http://dx.doi.org/10.1103/PhysRevB.80.014120.
[62] G.L.W. Hart, L.J. Nelson, R.W. Forcade, Generating derivative structures at a fixed concentration, Comput. Mater. Sci. 59 (2012) 101–107, http://dx.doi.org/10.1016/j.commatsci.2012.02.015.
[63] K.J. Michel, Y. Zhang, C. Wolverton, Fast mass transport kinetics in B20H16: a high-capacity hydrogen storage material, J. Phys. Chem. C 117 (2013) 19295–19301, http://dx.doi.org/10.1021/jp402669u.

Dr. Qianqian Li is an associate professor in Materials Genome Institute at Shanghai University, Shanghai, China. She received her BS degree in Materials Science and Technology from University of Jinan, Jinan, China in 2009, and her Ph.D. degree in solid mechanics from Zhejiang University, Hangzhou, China in 2014, and then followed to work as a postdoctoral research associate in NUANCE, Department of Materials Science and Engineering, at Northwestern University, Evanston, IL, USA, from 2014 to 2017. Her research area of interest includes *in-situ* transmission electron microscopy (TEM) and other related characterization tools, energy storage behaviors of electrodes for rechargeable batteries and supercapacitor, and synthesis and modification of functional materials.

Dr. Jinsong Wu is currently a research associate professor in Department of Materials Science and Engineering at the Northwestern University and TEM facility manager in the NU*ANCE* center. He earned his Ph.D. degree from the Department of Materials Science and Engineering at Dalian University of Technology, China. As an award winning microscopist, Dr. Wu's research interests include transmission electron microscopy, electron tomography, *in-situ* transmission electron microscopy and nanomaterials for energy storage.

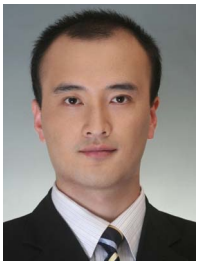

Dr. Zhenpeng Yao is currently a research assistant and Ph.D. student in Department of Materials Science and Engineering at the Northwestern University. He earned his M.S. degree from the Department of Mechanical Engineering at Shanghai Jiao Tong University, China. His research interests include first-principle studies on novel electrode materials and solid state electrolytes for rechargeable lithium and sodium-ion batteries.

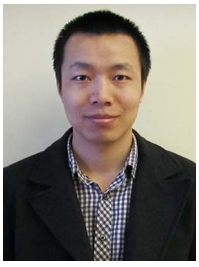

Dr. Yaobin Xu is a postdoctoral research associate in NUANCE, Department of Materials Science and Engineering, at Northwestern University, Evanston, IL, USA. He received a B.E. degree in Metallurgical Engineering from the Central South University in Changsha, China in 2010, and his Ph.D. degree in Materials Physics and Chemistry at the Shenyang National Laboratory for Materials Science, which is a part of the Institute of Metal Research of the Chinese Academy of Sciences in 2016. His research area of interest includes investigation of microstructures of ferroelectric thin films, electrodes for rechargeable batteries and catalysts by ex-situ and *in-situ* transmission electron microscopy (TEM).

Michael Thackeray is a Distinguished Fellow and senior scientist in the Electrochemical Energy Storage Department at Argonne National Laboratory. He received his Ph.D. from Cape Town University, South Africa and was a post-doctoral fellow at the Inorganic Chemistry Laboratory, Oxford University. He returned to South Africa to head the Battery Department at the Council of Scientific and Industrial Research before moving to Argonne in 1994. He is also Director of the US Department of Energy's Energy Frontier Research Center: The Center for Electrical Energy Storage. His principal research interests include the design of lithium battery electrode materials and their structure–electrochemical property relationships.

Chris Wolverton is a professor in the Materials Science Department at Northwestern University. Before joining the faculty, he worked at the Research and Innovation Center at Ford Motor Company. He received his BS degree in Physics from the University of Texas at Austin and his Ph.D. degree in Physics from the University of California at Berkeley, and performed postdoctoral work at the National Renewable Energy Laboratory (NREL). His research interests include computational studies of a variety of energy-efficient and environmentally friendly materials *via* first-principles atomistic and multiscale calculations. Professor Wolverton is a Fellow of the American Physical Society.

Prof. Vinayak P. Dravid is the Abraham Harris Chaired Professor of Materials Science & Engineering at and the founding director of the NU*ANCE* Center at Northwestern University. He received his Bachelor of Technology (B. Tech.) in Metallurgical Engineering from IIT Bombay, India; and Ph.D. in Materials Science and Engineering from Lehigh University. He has a diverse research portfolio encompassing advanced microscopy, nanotechnology, technology strategy, energy policy and emerging educational paradigms.